Published in final edited form as:
Magn Reson Med. 2012 June ; 67(6): 1827–1836. doi:10.1002/mrm.23196.

In Vivo Monitoring of pH, Redox Status, and Glutathione Using L-Band EPR for Assessment of Therapeutic Effectiveness in Solid Tumors

Andrey A. Bobko[1], **Timothy D. Eubank**[1], **Jeffrey L. Voorhees**[1], **Olga V. Efimova**[2], **Igor A. Kirilyuk**[3], **Sergey Petryakov**[2], **Dmitrii G. Trofimiov**[4], **Clay B. Marsh**[1], **Jay L. Zweier**[2], **Igor A. Grigor'ev**[3], **Alexandre Samouilov**[2], and **Valery V. Khramtsov**[1,*]

[1]Division of Pulmonary, Allergy, Critical Care, and Sleep Medicine, The Ohio State University, Columbus, Ohio, USA

[2]The Dorothy M. Davis Heart and Lung Research Institute, Division of Cardiovascular Medicine, Department of Internal Medicine, The Ohio State University, Columbus, Ohio, USA

[3]Vorozhtsov Institute of Organic Chemistry, Novosibirsk, Russia

[4]Novosibirsk State University, Novosibirsk, Russia

Abstract

Approach for in vivo real-time assessment of tumor tissue extracellular pH (pH_e), redox, and intracellular glutathione based on L-band EPR spectroscopy using dual function pH and redox nitroxide probe and disulfide nitroxide biradical, is described. These parameters were monitored in PyMT mice bearing breast cancer tumors during treatment with granulocyte macrophage colony-stimulating factor. It was observed that tumor pH_e is about 0.4 pH units lower than that in normal mammary gland tissue. Treatment with granulocyte macrophage colony-stimulating factor decreased the value of pH_e by 0.3 units compared with PBS control treatment. Tumor tissue reducing capacity and intracellular glutathione were elevated compared with normal mammary gland tissue. Granulocyte macrophage colony-stimulating factor treatment resulted in a decrease of the tumor tissue reducing capacity and intracellular glutathione content. In addition to spectroscopic studies, pH_e mapping was performed using recently proposed variable frequency proton–electron double-resonance imaging. The pH mapping superimposed with MRI image supports probe localization in mammary gland/tumor tissue, shows high heterogeneity of tumor tissue pH_e and a difference of about 0.4 pH units between average pH_e values in tumor and normal mammary gland. In summary, the developed multifunctional approach allows for in vivo, noninvasive pH_e, extracellular redox, and intracellular glutathione content monitoring during investigation of various therapeutic strategies for solid tumors. Magn Reson Med 000:000–000, 2011.

Keywords

solid tumors; bitroxides; glutathione; redox status; pH; L-Band EPR; PyMT mice; mammary gland; in vivo

*Correspondence to: Valery V. Khramtsov, Ph.D., 201 HLRI, 473 W 12th Avenue, The Ohio State University, Columbus, OH 43210. valery. khramtsov@osumc.edu.
AAB, TDE, AS, and VVK equally contributed to this work.

Additional Supporting Information may be found in the online version of this article

Tissue oxygenation, acidosis, redox, and glutathione (GSH) are among the most crucial parameters related to metabolism and physiology of tumors (1–5). Areas of hypoxia and acidosis are common features of solid neoplasia that have been well documented. Cells that exist in such adverse microenvironmental conditions can appreciably alter the tumor response to cytotoxic anticancer treatments. Indeed, it has been established that the presence of oxygen-deficient or hypoxic cells can not only lead to therapeutic resistance in preclinical tumor models but also have a detrimental effect on the ability to control human malignancies treated with curative intent. The acidic extracellular pH in tumors has a number of important consequences, playing a role in tumor initiation, progression, and therapy (2). Recently, pH_e has been identified as a significant prognostic factor not only in experimental transplantable tumor models but also in spontaneous tumors (6). Tumor cells are known to generate significant alterations in the redox status. This status is an important determinant in the response of the tumor to certain chemotherapeutic agents, radiation, and bioreductive hypoxic cell cytotoxins (4). Several studies have shown that GSH, a major contributor to intracellular redox status (7), is elevated in tumors (8,9). Intracellular GSH has been shown to be one of the major factors modulating tumor response to a variety of commonly used antineoplastic agents, including resistance toward cisplatin drugs (8). Therefore, development of approaches allowing for noninvasive assessment of these parameters in vivo provides an important tool for optimization of anticancer therapies and screening of anticancer drugs.

In the last decades, significant progress has been made regarding in vivo EPR techniques. L-band EPR instruments, designed to increase the depth of microwave penetration and decrease nonresonant losses, have become commercially available. Moreover, even lower-field (down to 250 MHz) homemade radiofrequency (RF) EPR spectrometers as well as instrumentation for spatial and spectral-spatial EPR imaging of radicals have been constructed at several EPR centers (10–12). The advances in pulsed EPR techniques operating at 300 MHz frequency allow for the first time in vivo imaging of nitroxides with narrow EPR lines (13). Alternatively, we recently proposed a functional proton–electron double-resonance imaging (PEDRI) approach allowing for functional mapping of the aqueous samples with high-quality MRI spatial resolution and short acquisition time using specially designed probes, e.g., pH mapping using pH-sensitive nitroxides (14,15). However, EPR-based techniques are far from attaining their maximum potential because of the lack of stable in vivo exogenous spin probes. This situation started to change for the better in recent years after development of a number of potentially useful paramagnetic probes for in vivo functional studies (16,17).

Here, we report an approach for in vivo tumor tissue multifunctional monitoring using L-band EPR-based techniques and specially designed paramagnetic probes. The approach allows for in vivo assessment of physiologically relevant tissue parameters, namely extracellular tissue acidity, redox, and intracellular GSH. In this study, we apply multifunctional EPR measurements in the model of breast cancer to assess changes of the tumor microenvironment induced by treatment with granulocyte macrophage colony-stimulating factor (GM-CSF) (18). In contrast to many anticancer agents, GM-CSF acts via recruiting more macrophages, also resulting in a fewer blood vessels and lower oxygen concentrations in tumors (18), which may affect tissue pH, redox, and GSH.

MATERIALS AND METHODS

Synthesis

The pH-sensitive spin probes R_1 and R_2 (see Fig. 1 for chemical structures) were synthesized as described in Supporting Information. The synthesis of the bis[(2,2,3,5,5-

pentamethyl-1-oxylimidazolidinyl-4)-methyl]-disulfide, RSSR, probe (Fig. 1) was performed as previously described (19).

Calibration of R_1 Nitroxide for pH Measurement by L-Band EPR Spectroscopy—Solutions of 1 mM nitroxide R_1 in a 2 mM Na-phosphate buffer, 150 mM NaCl were titrated with aliquots of HCl or NaOH to the required pH using a pH meter. EPR spectra of the samples were recorded in 1.5-mL centrifuge tubes using L-band EPR spectrometer (Magnettech, Germany). Hyperfine splitting constant (a_N) was measured as a half of the distance between low- and high-field components of the EPR spectra. Temperature was controlled using water bath attached to the thermostat.

Mice—Eight-week-old normal female FVB/N mice were purchased from the Jackson Laboratory. Late-stage mammary tumors from PyMT transgenic mice (MET-1 tumor cells) were removed and cultured for orthotopical injection into normal FVB/N female mice for these studies. Validation experiments of pH measurements by L-band EPR, variable radiofrequency (VRF) PEDRI, and electrochemical techniques were performed on untreated MET-1 tumors with average tumor volume of 4.1 cm^3 and normal mammary glands in wild-type C57Bl/6 mice.

Tumor Injections—MET-1 tumor cells were cultured in Dulbecco's Modified Eagle Medium (DMEM) containing 10% fetal bovine serum, 10 μg/mL insulin, and 5 ng/mL rhEGF. These cells were resuspended in DMEM medium at 500,000 cells/100 μL. The cells were orthotopically injected into the number four mammary fat pads of normal female FVB/N mice (allografts).

Treatment Strategy—After tumors became palpable (~0.2 cm^3), mice were randomized into treatment groups. Phosphate buffer saline (PBS) or rmGM-CSF (100 ng) in PBS (50 μL) was administered thrice per week intratumorally until the end of the trial (3 weeks). Tumor dimensions and mouse weights were measured three times per week. The assessment of extracellular pH and redox was performed using probe R_1 on the same animals (eight mice per group). GSH measurements were performed on separate set of animals (13 mice GMCSF/PBS treatment, 10 mice PBS treatment) using GSH-sensitive nitroxide RSSR. For GSH measurement, treatments were initiated 1 week after tumors became palpable.

In Vivo Electron Paramagnetic Resonance L-Band Studies—Mice were narcotized by inhalation of oxygen isoflurane mixture using Ohmeda Fluotec 3 anesthetic machine and then they were placed in the gap of L-band (1.2 GHz) EPR spectrometer (Magnettech, Germany). The surface coil resonator was firmly pressed into normal mammary glands or mammary tumors and spectrometer was tuned. Solutions of the R_1 probe in saline or RSSR probe in dimethylsulfoxide (10 μL, 10 mM) were injected intratissually for pH or GSH measurement, correspondingly. Immediately after injection, the EPR spectra were acquired for about 5 min. The kinetics of middle component intensity or distance between low-field and high-field component of EPR spectra of the R_1 probe were measured to determine reduction rate constants and pH, correspondingly. The kinetics of low-field component intensity of EPR spectra of RSSR probe were measured to calculate GSH concentration. The instrument settings were as follows: incident microwave power, 100 mW; modulation amplitude, 2.5 G; modulation frequency, 100 kHz; sweep width, 60 G; sweep time, 20 s (10 s for GSH measurements).

Validation of pH Measurements by L-Band EPR, VRF PEDRI, and Electrochemical Techniques—Measurements were performed on untreated MET-1 tumors with average tumor volume of 4.1 cm^3 and normal mammary glands in wild-type

C57Bl/6 mice. A pH microelectrode was inserted into the tumors or mammary glands using a 20-gauge needle (Warner Instruments, Hamden, CT) and tissue pH values were measured during 3-min intervals. Immediately after electrochemical measurements, mice were subjected to L-band (1.2 GHz) EPR pH studies in the same mammary glands or tumors. In the separate experiment, MET-1 tumor-bearing female C57Bl/6 mice were used to perform VRF PEDRI experiments for visualization of probe and pH values distribution within the tumors and mammary glands.

In Vivo PEDRI pH Mapping—PEDRI instrument was calibrated for R_2 paramagnetic probe as previously described (15). Namely, the phantom sample consisting of 10 glass tubes (400 μL volume, 32 mm long and 4 mm in diameter) filled with 1 mM R_2 solutions of various pH was used (schematically shown in Fig. 5a). Mice were narcotized as described above. Saline solutions of the R_2 probe (50 μL, 5 mM) were injected in tumor and mammary gland. Animal was placed into the PEDRI resonator assembly; resonators were tuned and then placed in the gap of the homemade PEDRI system. The images were acquired at 559.3 and 562.1 MHz frequencies of EPR irradiation and without EPR irradiation. The instrument settings were as follows: acquisition time for both PEDRI images, 16.8 s; repetition time, 2 s; echo time, 30 ms; matrix, 64 × 64; field of view, 100 × 100 mm^2; slice thickness, 20 mm; MRI acquisition time, 8.0 s; NMR frequency, 784.9 kHz. To find pH values, images acquired without EPR irradiation were subtracted from images obtained at two EPR frequencies and, the resulting images were divided pixel by pixel. pH values were calculated using calibration curve. Only significant pixels, with the signal enhancement exceeding 7-fold, were used for calculating the ratio which was plotted as a pH map.

Tissue Temperature Measurements—Tissue temperature was measured using Nomad Fiber Optic Thermometer (Neoptix, Canada) equipped with Fiber Optic Temperature Sensor with a probe diameter of 0.5 mm and precision of ± 0.2°C. The temperature probe was introduced in the normal mammary gland or mammary tumor using a sterile, stainless steel needle (gauge 18) at a depth approximately 3 mm from the tissue surface. The needle was then removed (leaving only the probe inserted into the tissue) to eliminate heat loss due to the heat conduction process through stainless steel.

Ex Vivo Analysis of GSH Content—Ex vivo analysis of GSH content in tumor and mammary gland tissues was performed as previously described (20) using the paramagnetic GSH-specific reagent, bis-(2,2,5,5)-tetramethyl-3-imidazoline-1-oxyl-4-yl) disulfide biradical (Enzo Life Sciences International, Inc., Plymouth Meeting, PA). Tumors and mammary glands were excised the day following the last in vivo EPR measurement and frozen in liquid nitrogen. Tissues were weighed and homogenized in the presence of 5-fold volume of PBS buffer containing 10 μL per mL Protease Inhibitor Cocktail III (AG Scientific, Inc., San Diego, CA; 5 mM Bestatin, 1.5 mM E-64, 100 mM AEBSF, HCl, 80 μM Aprotinin, 2 mM Leupeptin, 1 mM Pepstatin A), followed with 16,000 *g* centrifugation at 4°C for 5 min. The tissue supernatant was treated with 50 μM of the paramagnetic reagent (final concentration) at pH 7.0. EPR spectra were measured immediately after treatment. The label reacts with GSH in less than a second and shows a characteristic increase of the EPR triplet spectrum. The concentration of GSH was determined from a standard titration curve prepared with known concentrations of GSH under similar conditions as previously described (20).

Immunohistochemistry

The tumors were removed, fixed in formalin, sectioned, and stained for F4/80 (macrophages; Serotec, catalog # MCA497G), von Willebrand factor (blood vessels;

Abcam, catalog # ab6994), and Hypoxia-inducible factor (Hif-1α) (Santa Cruz, catalog # sc-53546) antigens.

RESULTS

Design of EPR Probes for In Vivo Monitoring of Tumor Tissue Extracellular pH

To be used for monitoring of tumor extracellular tissue acidosis, the spin pH probe has to (i) possess pH-sensitive spectral properties in the pH range from about 6.5 to 7.2, (ii) have enhanced stability to survive a reducing tumor microenvironment, and (iii) not penetrate cellular membranes to ensure probe targeting to extracellular space.

The imidazoline nitroxides were proven to be useful spin pH probes recently explored in several in vivo applications (21–23). They demonstrate strong pH effect on their EPR spectra due to protonation of the N-3 atom of the radical heterocycle (23). Recently, we developed the synthetic approaches allowing for pK_a adjustment (24) and enhancement of nitroxide stability toward reduction (22,25). It has been shown that binding of glutathione to the nitroxide label prevents nitroxide diffusion across the hydrophobic lipid bilayer of the biomembrane and therefore, enforces probe localization in extracellular aqueous volumes (26). In this study, we developed GSH-bound spin probe, R_1 (Fig. 1), with pK_a value being ideally fitted for detection of extracellular tumor tissue acidity (Fig. 2a). The bulky ethyl substitutes at positions 2 and 5 around the paramagnetic nitroxyl fragment of the R_1 are introduced to enhance its stability toward bioreduction (25). Note the comparatively broad linewidth of the EPR spectral lines of the radical R_1, ΔH_{pp} = 2.1 G, which primarily arises from unresolved hyperfine splittings with methelene protons (27). The deutero-substituted analog, R_2 (Fig. 1), has a significantly narrower linewidth, ΔH_{pp} = 1.2 G, and therefore higher spectral intensity. The EPR signal of the R_2 probe is easily saturated by RF irradiation which is of critical importance for PEDRI experiments (15). The detailed synthetic route for radicals R_1 and R_2 is described in Supporting Information. Figure 2a shows the typical EPR spectrum of the R_1 probe measured in vivo after intratumoral injection which corresponds to the acidic value of tumor pH_e, 6.52.

EPR Probes for In Vivo Monitoring of Tumor Redox State

Nitroxide reduction in biological systems into EPR silent products, predominantly hydroxylamines, provides information about tissue redox state (9,17). Ideally, nitroxide R_1 should be used as a dual function pH and redox probe, therefore minimizing invasiveness of the approach. Figure 2b shows the typical kinetics of R_1 reduction in the mammary gland and tumor clearly demonstrating a significant difference in reducing capacities of these tissues and functional sensitivity of the EPR approach using R_1 probe. Note that the R_1 probe is localized extracellularly and, therefore, provides information on extracellular redox of the tumor. Lower redox is known to be associated with a proliferating stage of the cell cycle. In general, intercellular redox signaling is related to both intracellular and extracellular redox statuses, therefore their measurements in tumor tissue might be of particular interest to elucidate the role of intercellular redox signaling in tumor progression.

EPR Probes for In Vivo Monitoring of Tumor Glutathione

During the last two decades, we developed GSH-specific paramagnetic analogs of Ellman's reagent (19,28) and recently demonstrated their applicability for in vivo intracellular GSH detection in ovarian tumor allograft in mice using L-band EPR spectroscopy (29). Figure 1 shows the chemical structure of the imidazoline disulfide biradical RSSR used in this study.

EPR spectra of RSSR are significantly affected by intramolecular spin exchange between two radical fragments resulting in appearance of "biradical" spectral components in addition

to the conventional triplet spectral pattern of the mononitroxide. Figure 3a demonstrates the typical changes of the EPR spectra of RSSR on addition of GSH. The decrease of biradical spectral components and simultaneous increase of monoradical components are consistent with splitting of the biradical disulfide bond due to its reaction with the GSH with the observed rate constant, k_{obs} (pH 7.2, 34°C) = 2.8 ± 0.2 M^{-1} s^{-1} (Fig. 3b). The RSSR label being a lipophilic compound diffuses easily across cellular membranes where it reacts with intracellular GSH providing a reliable EPR approach for determination of GSH in vitro (20) and in vivo (16,29). The approach is based on a dominant contribution of the GSH in the intracellular pool of fastreacting thiols. Fitting the initial part of the experimental kinetics of the EPR spectral change of the RSSR by the monoexponent allows for [GSH] determination (29).

In Vivo Multifunctional EPR Measurements

FVB/N female mice bearing MET-1 breast tumors were divided into three groups: untreated, treated with PBS, or PBS/GM-CSF. Figure 4a shows the timeline of tumor implantation, growth, and in vivo EPR measurements. Figure 4b shows the dependence of tumor growth on treatment illustrating significant slowing on PBS/GMCSF treatment compared with control PBS treatment or untreated tumors.

To study tumor microenvironment, the R_1 or RSSR probes were injected intratumorally and their L-band EPR spectra were measured during the next 10 min. The EPR spectra of the R_1 and RSSR probes were analyzed as described above to provide the values of extracellular tissue pH/redox, and intracellular GSH, correspondingly. Note that quantitative determinations of pH and [GSH] require calibration of the parameters of the probes, namely pK_a value of the R_1, and rate constant for the reaction of the RSSR with GSH, at the tissue temperature. Therefore, we performed tissue temperature measurements in the probe injection spot using a temperature-sensitive microsensor (see Materials and Methods section). The tissue temperatures both for normal mammary glands and tumors were found to be in the range 33.5–34.5°C. These values are slightly lower compared to the average mouse body temperature of 37°C apparently due to proximity of tissues to the surface and their underdeveloped microcirculation. The average value of 34°C has been used in further calculations. Calibration of the hyperfine splitting of the EPR spectra of the R_1 at various temperatures is shown in Figure 2a. The pK_a value for R_1 decreased 0.24 units when the temperature increased by 14°C and was estimated to equal 6.65 at 34°C. The calibration of the rate constant, k_{obs}, of the reaction of RSSR with GSH was performed at 34°C and pH 7.2 (see Fig. 3b).

In Vivo EPR Monitoring of Extracellular pH and Redox in MET-1 Tumors Using R_1 Probe

Figure 2 illustrates applicability of the R_1 probe to report tissue pH_e and redox. Simultaneous measurements using pH microelectrode and L-band EPR in the same tumor and normal mammary gland tissues showed comparable values of pH_e validating the EPR approach (see Table 1). To visualize probe localization and pH distribution within the tissue, we used recently developed functional PEDRI (14,30). In general, the PEDRI approach is based on MRI enhancement on EPR irradiation of paramagnetic probes resulted from a transfer of polarization from the electrons to protons by Overhauser effect (31–33), and therefore, it inherits high resolution, fast image acquisition, and availability of anatomical information of MRI technique. Functional PEDRI, namely variable field (14) and VRF (30) PEDRI (Fig. 5a) are based on MRI detection with EPR excitation at preselected EPR fields or frequencies, respectively. The use of a stationary magnetic field in VRF PEDRI results in elimination of field cycling and has an advantage over variable field PEDRI allowing for decrease of the acquisition time by exclusion periods of field ramping and stabilization. Improved field homogeneity and stability allow for the fast spin echo MRI acquisition.

Figure 5b shows tissue pH_e map obtained in living mouse after R_2 probe injections in tumor and in normal mammary gland. Two areas of probe localization correspond to tumor (left) and mammary gland (right) with higher pH heterogeneity in tumor compared with mammary gland. Average pH_e values in tumor and mammary gland were found to be in agreement with EPR spectroscopy and microelectrode data (see Table 1).

Figure 6 summarizes the data on pH_e and redox measurements. Tumor pH_e was found to be significantly lower than pH_e of the normal mammary gland (Fig. 6a). PBS treatment alone significantly increased pH_e. Buffer-induced increase of tumor tissue pH_e has been recently discussed in relation to inhibitory effects of systemic buffers on tumor growth (34,35; see also Fig. 4b). Treatment with GM-CSF/PBS significantly decreases tumor pH_e compared with control PBS treatment (Fig. 6a).

The extracellular reducing capacity of tumor tissue was found to be significantly higher compared with that of the normal mammary gland (Fig. 6b). Treatment of the tumor with GM-CSF/PBS but not PBS alone resulted in significant “normalization” of the tumor redox status. To elaborate whether GM-CSF-induced changes in tumor extracellular reducing capacity correlate with intracellular redox, we performed parallel in vivo measurements of tissue intracellular GSH.

In Vivo EPR Monitoring of Intracellular GSH in Tumor Tissue Using RSSR Probe

Figure 7a shows typical in vivo EPR spectra changes after RSSR intratumoral injection. The double integration of the EPR spectra measured immediately after probe injection and at the time point of maximal monoradical signal amplitude (150 s) shows insignificant, less than 10%, decay of the total EPR signal. Therefore, in first approximation, the initial exponential I_m increase can be described only by the reaction of RSSR with GSH neglecting contribution of the reduction. Figure 7b shows the representative kinetics of the monoradical spectral peak intensity change measured in mammary tumor and normal mammary gland of female FVB/N mice. The analysis of the kinetics allows for the evaluation of the intracellular GSH concentration being significantly higher in tumor, 10.7 mM, compared with that in mammary gland, 3.3 mM. As an additional validation of the in vivo approach, after in vivo studies GSH content was measured in vitro in tissue homogenates obtained from the sacrificed animals (see Materials and Methods section).

Figure 8 summarizes the data on in vivo and in vitro GSH measurements. The in vitro data represent the GSH content normalized to the total weight of the tissue sample while in vivo data represent average GSH concentrations in aqueous intracellular volume. Both in vivo and in vitro data show qualitatively agreeable several-fold larger GSH contents in tumors compared with normal mammary glands. Quantitative comparison of in vitro and in vivo data is difficult and requires knowledge of the relative intracellular aqueous volume of the total tissue volume. Note that relative total intracellular volumes on average are about 50% of the total tissue volume and may vary between normal and tumor tissues (36). Treatment with GM-CSF/PBS resulted in significant decrease of intracellular GSH measured in vivo, therefore supporting inter-relationship between extracellular and intracellular tumor redox states (cf. Figs. 6b and 8).

Phenotypical Changes of Murine Mammary Tumors

It has been shown GM-CSF treatment augments the number of tumor-residing macrophages, reduces tumor angiogenesis and oxygenation in a mouse model of breast cancer (18). Therefore, the tumors were resected at the end of the 3 week trial, sectioned, and subjected to the immunohistochemistry analysis. In the tumors treated with GM-CSF, we observe an increase in macrophage influx, a decrease in the number of von Willebrand factor (+) blood

vessels, and an increase in HIF-1α stabilization compared to the PBS-treated tumors (Fig. 9).

DISCUSSION

Tissue oxygenation, acidosis, redox, and glutathione are among the most crucial parameters of the tumor microenvironment related to metabolism and physiology of tumors (1–4). Variations in the tumor microenvironment may significantly modulate tumor progression, transition to malignancy, metastatic activity and effectiveness of anticancer therapies, and serve as significant prognostic factors of treatment outcome and survival. The accumulated data point to the importance of a noninvasive in vivo assessment of these parameters of tumor microenvironment to select the most appropriate and effective treatment strategy.

NMR and low-field EPR spectroscopic and imaging techniques have the advantage of in vivo applications in animals and humans due to sufficient depth of penetration in living tissue. While NMR and MRI have found broad clinical applications, EPR and EPRI biomedical applications are still in their infancy. The bottle-neck of many biological EPR applications is the requirement to have exogenous paramagnetic probes with high biostability, functional spectral sensitivity, and low toxicity. In return, the use of exogenous paramagnetic probes and lack of endogenous EPR signals provide EPR techniques with an advantage in signal specificity and functional sensitivity. In particularly, in vivo EPR was proven to be an effective method to monitor tumor tissue oxygenation and redox status (3,5,17,37–39).

A wide set of pH-sensitive nitroxides was developed to access the tissue acidity (23), including nitroxides with enhanced stability toward bioreduction (25) for use in vivo (16,22). EPR-measured rates of the nitroxide reduction depend on overall tissue redox status allowing for the differentiation of normal and pathological states, including reports on highly reducing tumor tissue microenvironment (3,9,17). The thiol-specific paramagnetic analogs of Ellman's reagent, disulfide nitroxide biradicals, were recently for the first time applied for intratumoral GSH assessment in living mice (29). These recent advances in functional paramagnetic probes and progress in low-field EPR-based techniques make biomedical multifunctional in vivo EPR applications feasible.

Measurement of extracellular pH provides a challenge for widely used ^{31}P NMR using endogenous phosphate which reports intracellular pH but is practically insensitive to pH_e (2). Therefore, the available MRI and NMR techniques for the measurement of tumor pH_e rely entirely on exogenous probes such as ^{31}P pH probe 3-aminopropylphosphate, ^{19}F pH probes triflouromethylated pyridoxal derivative and ZK-150471 (2), and hyperpolarized ^{13}C-labeled bicarbonate (40). A number of studies using microelectrodes, pH-sensitive MRI contrast agents, and hyperpolarized C-13 bicarbonate have consistently shown that the pH_e values of tumors, 6.5–7.0, are lower by 0.3– 0.5 units than that of healthy tissues, 7.1–7.4 (2,36,40). On application of exogenous probes, EPR spectroscopy has the advantage of higher sensitivity compared with NMR for the same probe concentration and higher probe stability compared with hyperpolarizing agents. In this study, we designed the pH-sensitive nitroxide R_1 and its deutero-substituted analog, R_2, for EPR monitoring of pH_e in tumors. Enhanced stability of the nitroxides R_1 and R_2, extracellular localization and sensitivity in the pH range of 6.5–7.5 allow for easy pH_e detection in EPR spectroscopic (Figs. 2a, 6a) and imaging (Fig. 5) applications while the rate of the reduction provides information on reducing capacity of tumor microenvironment (Figs. 2b and 6b). Applications of the nitroxides to access tissue redox status in vivo is a widely accepted concept (41) based on well-studied reduction of the nitroxides to the diamagnetic hydroxylamines by numerous biologically relevant reducing agents (ascorbic

acid, metals, quinones, redox-active enzymes, etc.) (42). The specific feature of R_1 probe is its highly hydrophilic character which specifies its extracellular localization. Extracellular tumor redox is apparently related to intracellular redox status, providing a mechanism for tumor cells to modulate intercellular redox signaling, and therefore affect tumor progression and therapy. In general, the redox measurements using R_1 nitroxide probe may be affected by differences in probe elimination by blood flow in normal and tumor tissues. While additional studies are required to answer this question, the larger R_1 signal decay rates observed in the tumors (characterized by underdeveloped vascularization) compared with the control mammary glands support a major contribution of the reduction in the signal decay. In imaging experiments, we did not observe significant probe distribution to the areas beyond tumor and mammary glands for 3–4 min after probe injection which is time window for redox measurements. The glutathione, presenting inside the cells in millimolar concentrations, is considered to be a major redox buffer and regulator of the intracellular redox status. Elevated level of GSH in tumors (9,29,43) hinders the effectiveness of many anticancer therapies. Detection of GSH in vivo using ^{1}H magnetic resonance spectroscopy is hindered by spectral overlap with other metabolites (43). Here, we applied recently developed application of disulfide nitroxide biradicals for in vivo intracellular tissue GSH assessment using L-band EPR technique (29).

Previously, we observed a significant decrease in tumor growth (Fig. 4b), angiogenesis, metastases, and pO_2 level on treatment with GM-CSF in a PyMT model of breast cancer (18). L-band EPR-measured tumor pH_e in this model of breast cancer was found to be about 0.5 units lower than pH_e of normal mammary glands (Fig. 6a). The spectroscopic measurements of pH_e were validated by microelectrode data and represent average pH_e of tumor as supported by pH mapping using VRF PEDRI (Fig. 5b). Note higher heterogeneity of the tumor acidity and higher contrast of low-field MRI image of tumor compared with normal mammary gland. The latter was previously reported for breast tumor imaging with ultralow-field MRI (44). The tumor reducing capacity measured by the reduction rate of the same probe R_1 (Fig. 6b) and tumor GSH (Fig. 8) measured using RSSR probe were found significantly elevated compared with that in normal mammary gland. PBS treatment alone did not affect tumor redox and GSH while significantly increased pH_e (Fig. 6a) and slowed tumor growth (Fig. 4b). The inhibitory effect of systemic buffers on tumor growth has been previously discussed in relation to buffer-induced improvement of tumor tissue pH homeostasis (34,35). On the contrary, treatment with GMCSF/PBS significantly decreases tumor pH_e (Fig. 6a) as well as redox (Fig. 6b) and intracellular GSH (Fig. 8) compared with control PBS treatment. This allows us to conclude that the GM-CSF/PBS inhibitory effect on tumor growth has a completely different mechanism.

We observed an increased number of macrophages in the tumors treated with GM-CSF (Fig. 9). Previously, it has been reported that the number of tumor-associated macrophages portends poor prognosis for patients with breast cancer (45) but the phenotype of these macrophages was not delineated. Recently, we have shown that local treatment of the tumor with GM-CSF results in the increased number of macrophages with an antitumor, M1, phenotype (18). These macrophages block vascular endothelial growth factor activity by producing soluble vascular endothelial growth factor receptor-1. Indeed, our data confirms that GM-CSF treatment reduces the number of blood vessels and induces hypoxic state within the tumors compared to the PBS treatment (Fig. 9). The observed decrease in tumor pH_e in response to GM-CSF is likely due to both the increased presence of macrophages coupled with change to an anaerobic metabolism in hypoxic regions resulting in acidosis build-up, and the maintenance of a more hypoxic environment driven by release of soluble vascular endothelial growth factor receptor- 1. An increased number of macrophages may be also responsible for the normalization of tumor GSH and redox (Figs. 6b and 8), potentially creating a more therapeutic- friendly environment.

In summary, multifunctional EPR-based approach allows for in vivo, noninvasive measurements of extracellular pH, redox, and intracellular GSH content in solid tumors. In combination with previously developed EPR oximetric applications to tumors, it significantly extends available capabilities for monitoring of tumor microenvironment during investigation of various therapeutic strategies. Among the immediate applications of this multifunctional approach is the animal testing of candidate anticancer drugs via in vivo quantification of their effects on tumor tissue parameters related to tumor growth and angiogenesis. This has potential to dramatically decrease the time required to identify novel therapeutics discerned through volumetric changes, thus speeding the development of these drugs into production, and ultimately to the clinic.

Supplementary Material

Refer to Web version on PubMed Central for supplementary material.

Acknowledgments

NIH; Grant numbers: EB009433, EB004900, CA132068, and HL089036; Grant sponsor: RFFI; Grant number: 10-04-91331.

References

1. Vaupel P, Mayer A. Hypoxia in cancer: significance and impact on clinical outcome. Cancer Metastasis Rev. 2007; 26:225–239. [PubMed: 17440684]
2. Gillies RJ, Raghunand N, Garcia-Martin ML, Gatenby RA. pH imaging. A review of pH measurement methods and applications in cancers. IEEE Eng Med Biol Mag. 2004; 23:57–64. [PubMed: 15565800]
3. Takeshita K, Kawaguchi K, Fujii-Aikawa K, Ueno M, Okazaki S, Ono M, Krishna MC, Kuppusamy P, Ozawa T, Ikota N. Heterogeneity of regional redox status and relation of the redox status to oxygenation in a tumor model, evaluated using electron paramagnetic resonance imaging. Cancer Res. 2010; 70:4133–4140. [PubMed: 20442282]
4. Cook JA, Gius D, Wink DA, Krishna MC, Russo A, Mitchell JB. Oxidative stress, redox, and the tumor microenvironment. Semin Radiat Oncol. 2004; 14:259–266. [PubMed: 15254869]
5. Halpern, HJ. Applications of in vivo EPR spectroscopy and imaging in cancer research. In: Berliner, LJ., editor. In vivo EPR (ESR): theory & applications. New York: Kluwer Academic/Plenum Publishers; 2003. p. 469-482.
6. Lora-Michiels M, Yu D, Sanders L, Poulson JM, Azuma C, Case B, Vujaskovic Z, Thrall DE, Charles HC, Dewhirst MW. Extracellular pH and P-31 magnetic resonance spectroscopic variables are related to outcome in canine soft tissue sarcomas treated with thermoradiotherapy. Clin Cancer Res. 2006; 12:5733–5740. [PubMed: 17020978]
7. Schafer FQ, Buettner GR. Redox environment of the cell as viewed through the redox state of the glutathione disulfide/glutathione couple. Free Radic Biol Med. 2001; 30:1191–1212. [PubMed: 11368918]
8. Rabik CA, Dolan ME. Molecular mechanisms of resistance and toxicity associated with platinating agents. Cancer Treat Rev. 2007; 33:9–23. [PubMed: 17084534]
9. Kuppusamy P, Li H, Ilangovan G, Cardounel AJ, Zweier JL, Yamada K, Krishna MC, Mitchell JB. Noninvasive imaging of tumor redox status and its modification by tissue glutathione levels. Cancer Res. 2002; 62:307–312. [PubMed: 11782393]
10. He G, Samouilov A, Kuppusamy P, Zweier JL. In vivo imaging of free radicals: applications from mouse to man. Mol Cell Biochem. 2002; 234–235:359–367.
11. Elas M, Williams BB, Parasca A, Mailer C, Pelizzari CA, Lewis MA, River JN, Karczmar GS, Barth ED, Halpern HJ. Quantitative tumor oxymetric images from 4D electron paramagnetic resonance imaging (EPRI): methodology and comparison with blood oxygen level-dependent (BOLD) MRI. Magn Reson Med. 2003; 49:682–691. [PubMed: 12652539]

12. Lurie DJ. Free radical imaging. Br J Radiol. 2001; 74:782–784. [PubMed: 11560824]
13. Hyodo F, Matsumoto S, Devasahayam N, Dharmaraj C, Subramanian S, Mitchell JB, Krishna MC. Pulsed EPR imaging of nitroxides in mice. J Magn Reson. 2009; 197:181–185. [PubMed: 19157932]
14. Khramtsov VV, Caia GL, Shet K, Kesselring E, Petryakov S, Zweier JL, Samouilov A. Variable field proton-electron double-resonance imaging: application to pH mapping of aqueous samples. J Magn Reson. 2010; 202:267–273. [PubMed: 20007019]
15. Efimova OV, Sun Z, Petryakov S, Kesselring E, Caia GL, Johnson D, Zweier JL, Khramtsov VV, Samouilov A. Variable radio frequency proton-electron double-resonance imaging: application to pH mapping of aqueous samples. J Magn Reson. 2011; 209:227–232. [PubMed: 21320790]
16. Khramtsov, VV.; Zweier, JL. Functional in vivo EPR spectroscopy and imaging using nitroxide and trityl radicals. In: Hicks, R., editor. Stable radicals: fundamentals and applied aspects of odd-electron compounds. Chichester, UK: Wiley; 2010. p. 537-566.
17. Davis RM, Mitchell JB, Krishna MC. Nitroxides as cancer imaging agents. Anticancer Agents Med Chem. 2011; 11:347–358. [PubMed: 21434855]
18. Eubank TD, Roberts RD, Khan M, Curry JM, Nuovo GJ, Kuppusamy P, Marsh CB. Granulocyte macrophage colony-stimulating factor inhibits breast cancer growth and metastasis by invoking an antiangiogenic program in tumor-educated macrophages. Cancer Res. 2009; 69:2133–2140. [PubMed: 19223554]
19. Khramtsov VV, Yelinova VI, Glazachev Yu I, Reznikov VA, Zimmer G. Quantitative determination and reversible modification of thiols using imidazolidine biradical disulfide label. J Biochem Biophys Methods. 1997; 35:115–128. [PubMed: 9350517]
20. Nohl H, Stolze K, Weiner LM. Noninvasive measurement of thiol levels in cells and isolated organs. Methods Enzymol. 1995; 251:191–203. [PubMed: 7651197]
21. Mader K, Gallez B, Liu KJ, Swartz HM. Non-invasive in vivo characterization of release processes in biodegradable polymers by low-frequency electron paramagnetic resonance spectroscopy. Biomaterials. 1996; 17:457–461. [PubMed: 8938242]
22. Potapenko DI, Foster MA, Lurie DJ, Kirilyuk IA, Hutchison JM, Grigor'ev IA, Bagryanskaya EG, Khramtsov VV. Real-time monitoring of drug-induced changes in the stomach acidity of living rats using improved pH-sensitive nitroxides and low-field EPR techniques. J Magn Reson. 2006; 182:1–11. [PubMed: 16798033]
23. Khramtsov VV. Biological imaging and spectroscopy of pH. Curr Org Chem. 2005; 9:909–923.
24. Kirilyuk IA, Shevelev TG, Morozov DA, Khromovskih EL, Skuridin NG, Khramtsov VV, Grigor'ev IA. Grignard reagent addition to 5-alkylamino- 4*H*-imidazol 3-oxdes: synthesis of new pH-sensitive spin probes. Synthesis. 2003; 6:871–878.
25. Kirilyuk IA, Bobko AA, Grigor'ev IA, Khramtsov VV. Synthesis of the tetraethyl substituted pH-sensitive nitroxides of imidazole series with enhanced stability towards reduction. Org Biomol Chem. 2004; 2:1025–1030. [PubMed: 15034626]
26. Woldman YY, Semenov SV, Bobko AA, Kirilyuk IA, Polienko JF, Voinov MA, Bagryanskaya EG, Khramtsov VV. Design of liposomebased pH sensitive nanoSPIN probes: nano-sized particles with incorporated nitroxides. Analyst. 2009; 134:904–910. [PubMed: 19381383]
27. Bobko AA, Kirilyuk IA, Gritsan NP, Polovyanenko DN, Grigor'ev IA, Khramtsov VV, Bagryanskaya EG. EPR and quantum chemical studies of the pH-sensitive imidazoline and imidazolidine nitroxides with bulky substituents. Appl Magn Reson. 2010; 39:437–451. [PubMed: 22162912]
28. Khramtsov VV, Yelinova VI, Weiner LM, Berezina TA, Martin VV, Volodarsky LB. Quantitative determination of SH groups in low- and high-molecular-weight compounds by an electron spin resonance method. Anal Biochem. 1989; 182:58–63. [PubMed: 2557778]
29. Roshchupkina GI, Bobko AA, Bratasz A, Reznikov VA, Kuppusamy P, Khramtsov VV. In vivo EPR measurement of glutathione in tumorbearing mice using improved disulfide biradical probe. Free Radic Biol Med. 2008; 45:312–320. [PubMed: 18468522]
30. Efimova OV, Sun Z, Petryakov S, Kesselring E, Caia GL, Johnson D, Zweier JL, Khramtsov VV, Samouilov A. Variable radio frequency proton-electron double-resonance imaging: application to pH mapping of aqueous samples. J Magn Reson. 2011; 209:227–232. [PubMed: 21320790]

31. Lurie DJ, Bussell DM, Bell LH, Mallard JR. Proton electron double magnetic resonance imaging of free radical solutions. J Magn Reson. 1988; 76:366–370.
32. Ardenkjaer-Larsen JH, Laursen I, Leunbach I, Ehnholm G, Wistrand LG, Petersson JS, Golman K. EPR and DNP properties of certain novel single electron contrast agents intended for oximetric imaging. J Magn Reson. 1998; 133:1–12. [PubMed: 9654463]
33. Golman K, Leunbach I, Ardenkjaer-Larsen JH, Ehnholm GJ, Wistrand LG, Petersson JS, Jarvi A, Vahasalo S. Overhauser-enhanced MR imaging (OMRI). Acta Radiol. 1998; 39:10–17. [PubMed: 9498861]
34. Robey IF, Baggett BK, Kirkpatrick ND, Roe DJ, Dosescu J, Sloane BF, Hashim AI, Morse DL, Raghunand N, Gatenby RA, Gillies RJ. Bicarbonate increases tumor pH and inhibits spontaneous metastases. Cancer Res. 2009; 69:2260–2268. [PubMed: 19276390]
35. Silva AS, Yunes JA, Gillies RJ, Gatenby RA. The potential role of systemic buffers in reducing intratumoral extracellular pH and acidmediated invasion. Cancer Res. 2009; 69:2677–2684. [PubMed: 19276380]
36. Vaupel, P. Pathophysiology of solid tumors. In: Molls, M.; Vaupel, P.; Nieder, C.; Anscher, MS., editors. The impact of tumor biology on cancer treatment and multidisciplinary strategies. Berlin, Heidelberg: Springer; 2009. p. 51-92.
37. Halpern HJ, Yu C, Peric M, Barth E, Grdina DJ, Teicher BA. Oxymetry deep in tissues with low-frequency electron paramagnetic resonance. Proc Natl Acad Sci U S A. 1994; 91:13047–13051. [PubMed: 7809170]
38. Khan N, Williams BB, Hou H, Li H, Swartz HM. Repetitive tissue pO2 measurements by electron paramagnetic resonance oximetry: current status and future potential for experimental and clinical studies. Antioxid Redox Signal. 2007; 9:1169–1182. [PubMed: 17536960]
39. Diepart C, Jordan BF, Gallez B. A New EPR oximetry protocol to estimate the tissue oxygen consumption in vivo. Radiat Res. 2009; 172:220–225. [PubMed: 19630526]
40. Gallagher FA, Kettunen MI, Day SE, Hu DE, Ardenkjaer-Larsen JH, Zandt R, Jensen PR, Karlsson M, Golman K, Lerche MH, Brindle KM. Magnetic resonance imaging of pH in vivo using hyperpolarized 13Clabelled bicarbonate. Nature. 2008; 453:940–943. [PubMed: 18509335]
41. Matsumoto K, Hyodo F, Matsumoto A, Koretsky AP, Sowers AL, Mitchell JB, Krishna MC. High-resolution mapping of tumor redox status by magnetic resonance imaging using nitroxides as redox-sensitive contrast agents. Clin Cancer Res. 2006; 12:2455–2462. [PubMed: 16638852]
42. Kocherginsky, N.; Swartz, HM. Nitroxide spin labels. Reactions in biology and chemistry. Boca Raton, New York, London, Tokyo: CRC Press; 1995. p. 270
43. Opstad KS, Provencher SW, Bell BA, Griffiths JR, Howe FA. Detection of elevated glutathione in meningiomas by quantitative in vivo 1H MRS. Magn Reson Med. 2003; 49:632–637. [PubMed: 12652533]
44. Dean KI, Komu M. Breast tumor imaging with ultra low field MRI. Magn Reson Imaging. 1994; 12:395–401. [PubMed: 8007768]
45. Leek RD, Lewis CE, Whitehouse R, Greenall M, Clarke J, Harris AL. Association of macrophage infiltration with angiogenesis and prognosis in invasive breast carcinoma. Cancer Res. 1996; 56:4625–4629. [PubMed: 8840975]

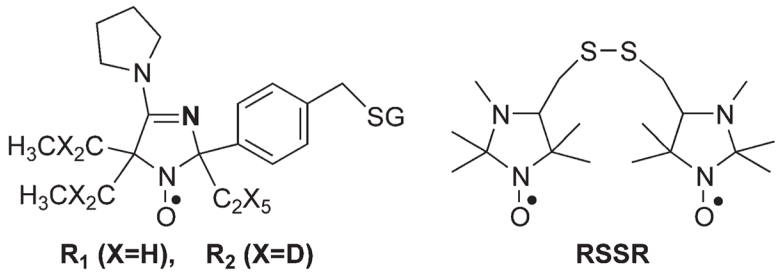

FIG. 1.
The chemical structure of the paramagnetic probes R_1, R_2, and RSSR.

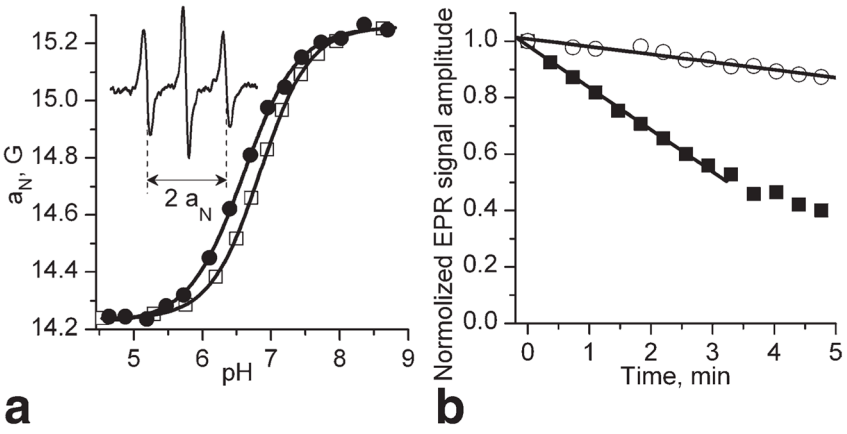

FIG. 2.

a: pH dependencies of the hyperfine splitting, a_N, for R_1 probe measured using L-band EPR spectroscopy. Temperature-dependent shift of the titration curve was observed with pK_a values being equal to 6.84 (□, 23°C) and 6.60 (●, 37°C). Insert: L-band EPR spectrum of the R_1 probe measured in vivo after injection (10 μL, 10 mM) in mammary tumor tissue. The hyperfine splitting, a_N, was found to be equal to 14.72 G which corresponds to the value of pH_e = 6.52 assuming tumor tissue temperature 34°C and pK_a = 6.65. **b**: EPR signal decay of the probe R_1 after injection (10 μL, 10 mM) in mammary glands (○) and mammary tumors (■). The analysis of the initial part of the kinetics yields the rates of the EPR signal reduction, k_{red}, in extracellular media of the tissues being equal to 0.5×10^{-3} s^{-1} and 2.5×10^{-3} s^{-1}, respectively.

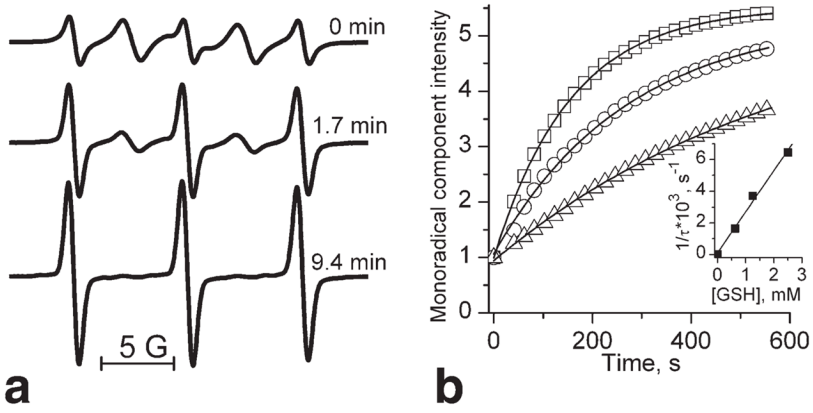

FIG. 3.

a: The EPR spectra of 100 μM RSSR measured at various time points after incubation with 2.5 mM GSH in 0.1 M Na-phosphate buffer, pH 7.2, and 1 mM DTPA at 34°C. **b**: The kinetics of the increase of amplitude of low-field monoradical component of the EPR spectrum after addition of various concentrations of GSH: 0.625 mM (△), 1.25 mM (○) and 2.5 mM (□). Lines represent the best fit of the experimental kinetics to the monoexponents. Inserts: The dependence of inverse time constant of the exponential kinetics, $1/\tau$, on GSH concentration. The linear regression ($1/\tau = k_{obs} \times [GSH]$) provides the observed rate constant value of the reaction between GSH and RSSR, k_{obs} (pH 7.2, 34°C) = 2.8 ± 0.2 M^{-1} s^{-1}.

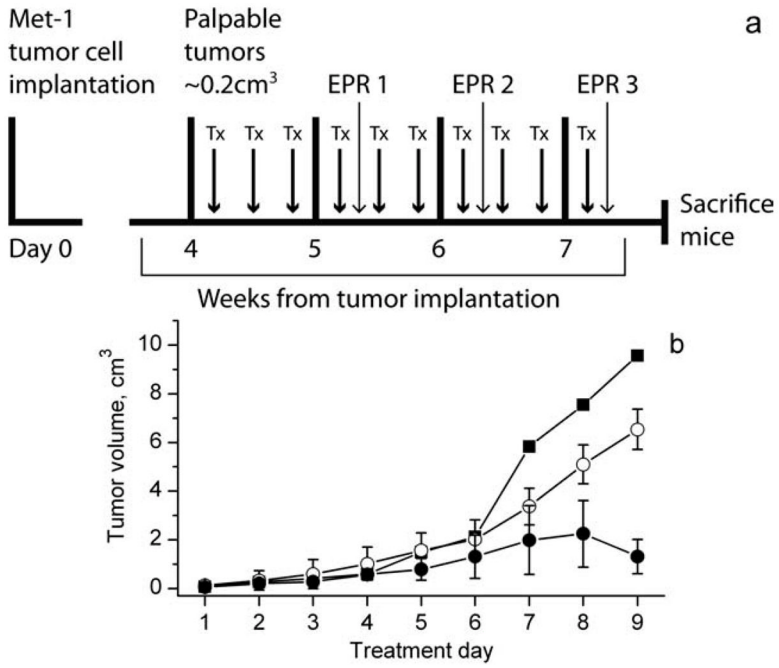

FIG. 4.

a: The timeline of the tumor implantation, treatment (Tx), and in vivo EPR measurements.

b: Tumor growth measured in FVB/N female mice bearing MET-1 breast cancer tumors: untreated tumors (■); treated with PBS (○) or GM-CSF/PBS (●).

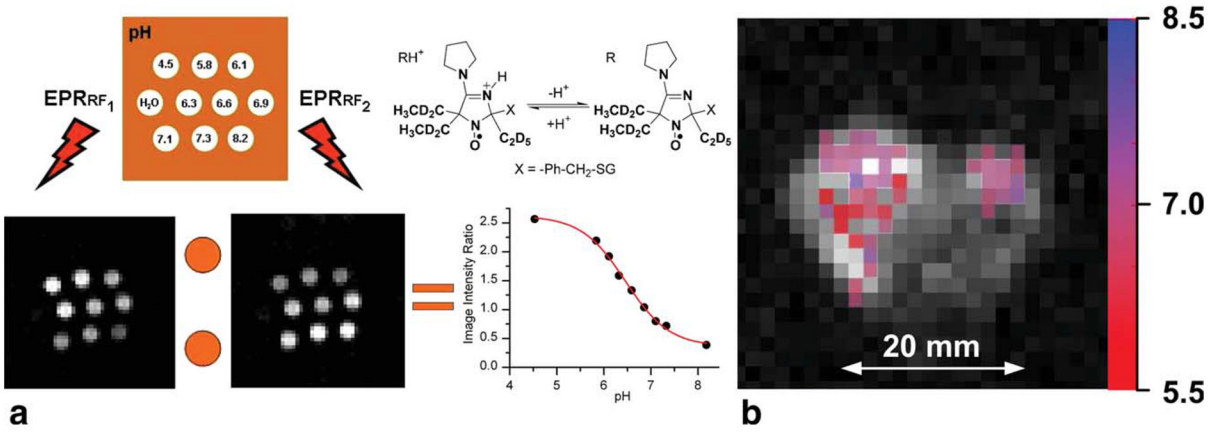

FIG. 5.

a: Illustration of VRF PEDRI application for pH-mapping. Two PEDRI images of the phantom were acquired during EPR irradiation (8.4 s) at two frequencies which correspond to EPR resonances of RH^+ and R forms of pH probe, R_2. Calibration curve was calculated as pH dependence of the ratio of signal amplitudes, $I(RF_1)/I(RF_2)$ (see Materials and Methods section). **b**: Extracellular pH mapping of living mice by VRF PEDRI. pH map (in color) was superimposed with low-field MRI (gray scale) showing the transversal view of the mouse. The R_2 probe was injected into the number 4 mammary gland containing the tumor (left) and in the number 9 normal mammary gland (right) before PEDRI/MRI acquisitions. The area of probe distribution in tumor is about 1 cm^2, which is significantly less than the cross-section area of the tumor, about 3 cm^2 (the measured tumor volume is 4.1 cm^3), therefore supporting probe distribution within the tumor. The corresponding area of probe distribution in mammary gland is less than 0.2 cm^2 which is comparable with the mammary gland size. The pH map was calculated from two PEDRI images, acquired during EPR irradiation at two frequencies. Total acquisition was 24.8 s with 16.8 s of EPR irradiation.

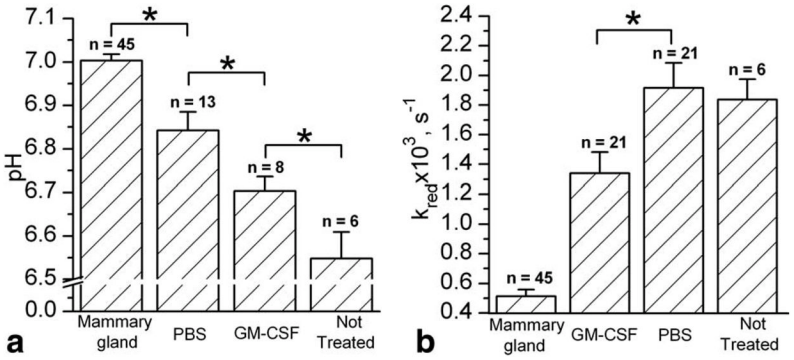

FIG. 6.

a: Tissue pH_e values of normal mammary gland and mammary tumors of female FVB/N mice measured by in vivo EPR. pH values were calculated for PBS-, GM-CSF/PBS-treated, and untreated tumors with volume greater than 1.2 cm^3 (*$P < 0.03$). **b**: The reduction rate of R_1 nitroxide, k_{red}, in extracellular media of normal mammary glands and variously treated tumors (*$P < 0.02$). Error bars denote standard error.

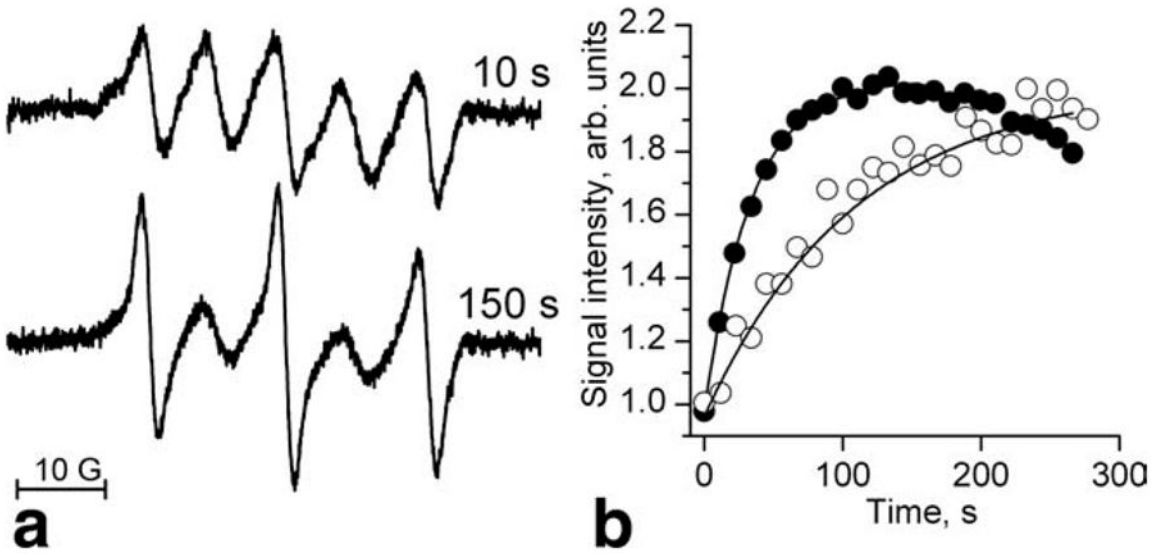

FIG. 7.

a: L-band EPR spectra of the RSSR radical measured in vivo in mammary tumor of female FVB/N mice 10 s and 150 s after probe injection. **b**: Kinetics of the monoradical spectral peak intensity change measured in mammary tumor (●) and normal mammary gland (○). The solid lines are the fits of the initial part of the kinetics by the monoexponent $I_m(t)=I_m^{max} - (I_m^{max} - I_m^{t=0})\exp(-k_{obs}[GSH] \cdot t$ supposing k_{obs} (pH 7.2, 34°C) = 2.8 M^{-1} s^{-1} and yielding [GSH] = 10.7 and 3.3 mM for the tumor and mammary gland, correspondingly.

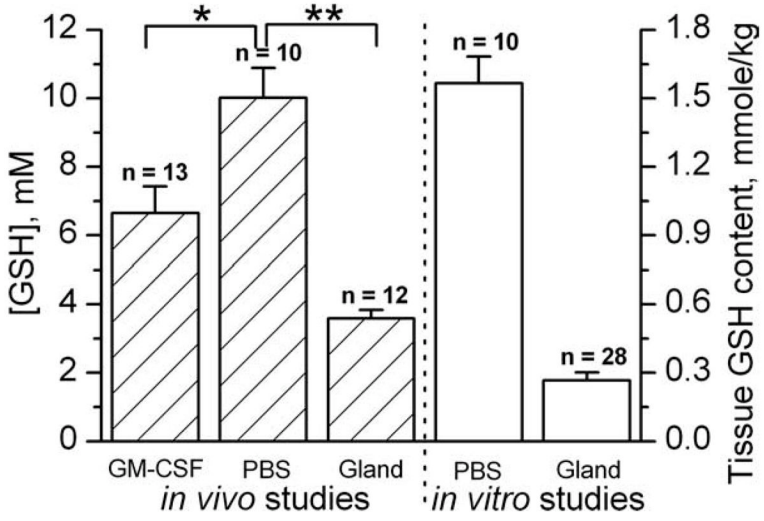

FIG. 8.

Intracellular GSH concentrations measured by in vivo EPR using RSSR probe, and tissue GSH contents measured in vitro (see Materials and Methods section) in the normal mammary glands and mammary tumors (>4.5 cm^3 volume) of female FVB/N mice (*$P <$ 0.01, **$P < 0.002$). Error bars denote standard error.

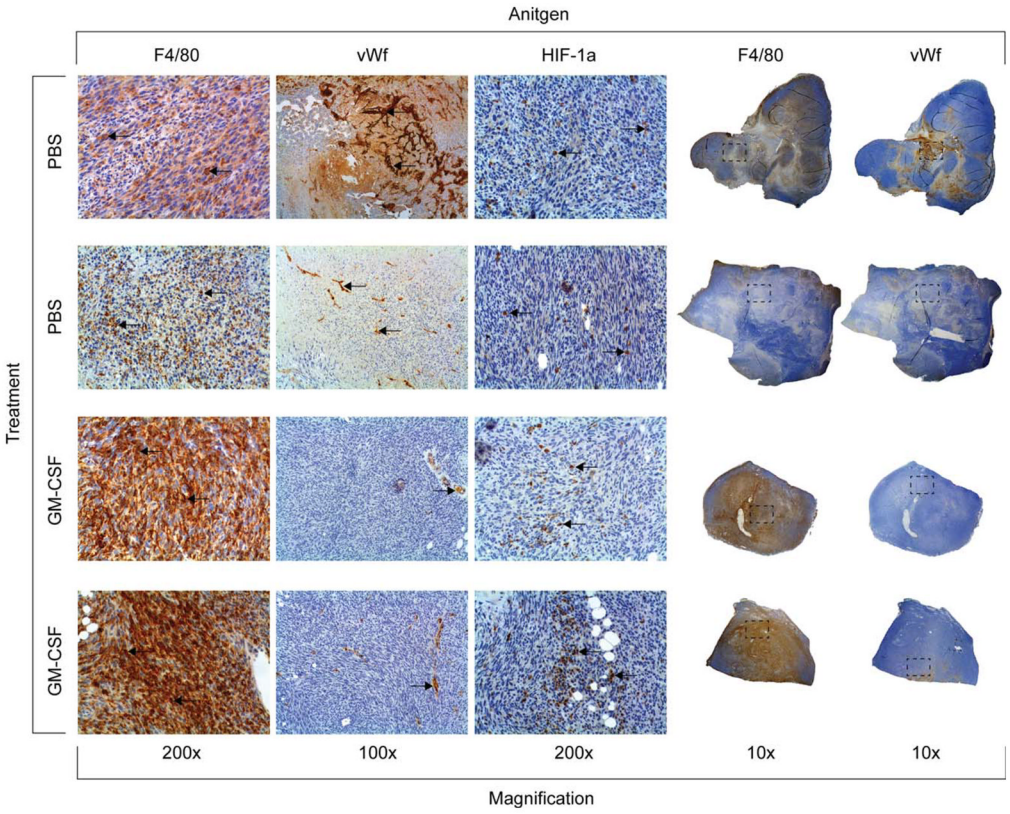

FIG. 9.

Phenotypical change of murine mammary tumors induced by treatment with GM-CSF. The tumors were removed after the final EPR measurement, sectioned, and stained for the presence of tumor macrophages (F4/80 antigen), blood vessels (von Willebrand factor antigen), or for the presence of HIF-1α. The PBS-treated tumors have less tumor macrophages, increased blood vessels, and less HIF-1α than those tumors treated with GM-CSF. [Color figure can be viewed in the online issue, which is available at wileyonlinelibrary.com.]

Table 1

Average pH Values Measured in Tumor and Mammary Gland Tissues in Wild-Type C57Bl/6 Mice Using Different Techniques

	pH values measured in tumors and mammary glands		
	L-band EPR	**pH microelectrode**	**VRF PEDRI**
Tumor	6.60 ± 0.07 (n = 3)	6.70 ± 0.05 (n = 3)	6.7 ± 0.1
Gland	6.98 ± 0.05 (n = 3)	7.01 ± 0.05 (n = 3)	7.1 ± 0.1